Electrical Power and Energy Systems 155 (2024) 109674

Contents lists available at ScienceDirect

International Journal of Electrical Power and Energy Systems

journal homepage: www.elsevier.com/locate/ijepes

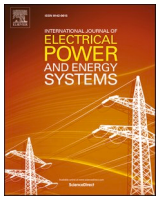

Disturbance size estimation in Great Britain power system including combined cycle gas turbine power stations

Rasoul Azizipanah-Abarghooee [a], Mostafa Malekpour [a], Rafat Aljarrah [b], Mazaher Karimi [c,*], Vladimir Terzija [d]

[a] Green Energy and Mobility Department, RINA Tech UK Ltd, Manchester, UK
[b] Electrical Engineering Department, Princess Sumaya University for Technology, Amman 1941, Jordan
[c] School of Technology and Innovations, University of Vaasa, Vaasa, Finland
[d] School of Engineering, Merz Court E4.41, Newcastle University, UK

ARTICLE INFO

Keywords:
Combined-cycle gas turbine (CCGT)
Disturbance size estimation
Frequency response
Great Britain

ABSTRACT

With the substantial popularity of combined cycle gas turbine (CCGT) power plants in the nowadays power systems, special care must be taken to regulate frequency due to unique frequency response characteristic of the full-loaded CCGT units. This unique feature is documented in the literature; however, its effect on determining frequency response of the power systems was not addressed in detail. This study proposes a new analytical method to achieve a more accurate estimated size of a loss-of-generation disturbance. This method considers demand-side power deviations and transmission lines power loss as well as unique frequency response of the CCGT units following the event. Firstly, it is exposed that there is an approximately linear relationship between power and frequency deviations of these plants in a real-world power system despite the complexity of the CCGT model. This relationship may be represented by a negative droop gain. Next, the derived CCGT's linear characteristic is formulated in the disturbance size estimation process. Finally, the effectiveness of the proposed modifications is demonstrated through extensive simulations on a 36-zone Great Britain equivalent test system.

1. Introduction

Combined cycle gas turbines (CCGTs) are one of the most favourable options for industrial sectors and power systems operators of many countries like United Kingdom. They can alleviate system costs and emissions due to their high efficiency and low greenhouse gas pollutions [1]. However, their unique frequency response characteristics can considerably affect the power systems stability following the abrupt disturbances. Since, it is a challenge to estimate the size of the power outage after frequency decay in the CCGT integrated networks as their output powers are functions of frequency deviation. Thus, sufficiently accurate disturbance size estimation schemes are required. A motivation for this study arises from the Enhanced Frequency Control Capability project, in which CCGT power stations is considered based on Gone Green 2020 planning and loss of generation size estimation is one of the most important steps in its smart frequency control procedure [2]. Moreover, optimization and allocation of spinning reserve can provide considerable cost reductions for power system operators [3,4].

The dynamic behaviour of CCGTs following a disturbance is widely explored and potential stability problems are highlighted under their full-load operation mode [5–8]. Moreover, during the last decade, there have been growing numbers of works on estimating disturbance size in terms of under-frequency load shedding based on the magnitude of the disturbance [9–12]. However, no attention has been placed on generation lost estimation once CCGT technologies have considerable penetration levels in power systems. The major challenge is that the discrepancy between frequency response characteristics of CCGTs and other conventional generation technologies is not yet stablished. This is because there is no relationship for frequency excursion and CCGTs power variations.

The unique frequency response of CCGTs leads to power systems stability issues since their output power operating at base or near-base load decreases following the frequency reduction events [6–8]. This is because that the compressor airflow reduces and thus temperature of hot air exhausted from gas turbine increases. As a result, the power output of CCGT is unexpectedly decreased due to the fuel reduction in order to limit exhaust temperature. An improved control strategy is proposed in [13] to ensure a better frequency regulation performance and keep the

* Corresponding author.
E-mail address: Mazaher.karimi@uwasa.fi (M. Karimi).

https://doi.org/10.1016/j.ijepes.2023.109674
Received 7 May 2023; Received in revised form 7 October 2023; Accepted 19 November 2023
Available online 25 November 2023

internal CCGT parameters within the non-violent operational modes. However, its effect on determining the frequency response of the power systems is not addressed in detail.

Speaking of disturbance size estimation, an adaptive under-frequency load shedding is presented in [9] to enhance the conventional technique. A load shedding strategy based on system frequency response is introduced in [10] for active power deficit estimation based on the initial rate-of-change-of-frequency (RoCoF) after the disturbance. An adaptive mechanism is proposed in [11] to specify the amount of disturbance size deploying under-frequency relays and observed initial ramp of the frequency decay. Another adaptive approach is introduced in [12] to determine the amount of load shedding or disturbance size using RoCoF information. However, instead of a generation outage, the study focuses on loss of load contingencies. Moreover, the frequency and voltage dependencies of loads are neglected. Additionally, the impact of post-event system's loss power variation on the infeed loss size estimation was ignored [14]. Recently, some researchers used generalized injection shift factors (ISF) to estimate transmission line flows during the transient period following a loss of generation or increase in load contingency [15,16]. The lines power deviation in the ISF methods are estimated through linearization of the system's offline power flow model. Although, neither the loads power deviation nor the CCGTs power reduction was considered.

In this study, our proposal is to utilize the primary frequency controller operation of the CCGTs and other generation units to determine the output power variation of frequency control supportive units. This paper derives a novel analytical approach using energy conservation law in order to improve the accuracy of the estimated value of lost power. In this regard, the post-event variations in the transmission power loss and the system's demand are formulated and improvised in the estimation process. In the case of the CCGTs, it is revealed that their power output has an approximately linear relationship with post-event steady-state frequency regardless of their non-linear dynamic behavior. This relationship can be represented by a negative droop gain. It is demonstrated that deploying this relationship can significantly mitigate the disturbance size estimation error. Finally, the effectiveness of the proposed approach is verified by a real-world 36-zone Great Britain equivalent power system implemented in DIgSILENT PowerFactory software. In particular, three different operational scenarios are analyzed to simulate discrepant CCGTs' installed capacities. These scenarios model the Great Britain system without CCGTs, with 60 % and 40 % of the system demand supplied by the CCGT units to simulate the possible configurations of CCGT and non-CCGT power stations. Extensive simulation results on different sizes of loss-of-generation contingencies illustrate that the presented modifications significantly improve the accuracy of the estimated disturbance size. Additionally, the results show that the CCGTs' droop gain is proportional to their installed capacity. To the best of our knowledge, this problem has not been dealt with by such a low-demanding and yet accurate approach in literature.

In the next section, a sensitivity analysis on various deficits is presented to obtain the power-frequency characteristic of a full load CCGT. The novel analytical formulation of impact of the CCGTs, frequency and voltage dependencies of load, load damping coefficient, and variation in the transmission line's losses on the disturbance size estimation is elaborated in Section 3. After the evaluation of the results using 36-zone multi-machine GB network in Section 4, the conclusions are drawn in Section 5.

2. Power-Frequency characteristic of combined cycle gas turbines

This section presents a dynamic model of the CCGT power stations, firstly. Then, a relationship between the amount of power reduction of a full-loaded CCGT and its frequency reduction, at post-event steady-state condition, is derived.

2.1. Combined cycle gas turbine modelling

The CCGT modelling for power system dynamic studies has been fully addressed in [5–8,13,17,18]. The structure of the studied combined cycle gas turbine model used in this study is illustrated in Fig. 1. In this model, the variables F_1 to F_3 are defined as follows [5]:

$$F_1 = T_R - A\left(1 - W_f\right) + B(1 - \omega_r) \tag{1}$$

$$F_2 = K_v^{-1}\left(W_f - F_{nl}\right) + 0.5(1 - \omega_r) \tag{2}$$

$$F_3 = \omega_r V^{0.257} \tag{3}$$

with ω_r, T_R, W_f, K_v, F_{nl}, and V as turbine speed, reference temperature, fuel flow, torque coefficient, no-load fuel, and inlet guide vane (IGV) position, respectively. Other parameters of the studied CCGT model are listed in Table 1. There are three key control loops on the CCGT model: compressor IGV control, temperature control and fuel control [5]. The hot exhaust gas of the gas turbine (GT) is fed into a heat recovery steam generator (HRSG) that can produce steam for steam turbine (ST) driving [19].

In this model, the mechanical power generated by the CCGT is calculated as:

$$P_m = K_{st}P_{st} + (1 - K_{st})P_{gt} \tag{4}$$

where, P_{gt} and P_{st} are GT power and ST power, respectively. Fig. 2 outlines the HRSG model in which Q_g is defined as:

$$Q_g = 0.9P_{gt} + 0.1 \tag{5}$$

The GT reference power $P_{gt,ref}$ may be modulated using a governor. If a frequency drop is occurred when the CCGT is operating at a rated condition, the exhaust temperature T_{ex} will be increased due to turbine speed and compressor speed reduction. In this condition, the IGV controls the airflow to bring the temperature back to the rated value which in turn decreases the CCGT's power P_m. In other words, this unique behavior of CCGTs changes the system frequency response particularly while their installed capacity is considerable.

2.2. The power-frequency characteristic of the CCGT

Deriving a closed-form relation between the CCGT power reduction and its frequency reduction is a very complicated task due to the complexity of the CCGT model. Accordingly, a new method is proposed to approximately determine the CCGT's power reduction in response to its frequency reduction. To this end, the studied CCGT's responses for different frequency excursions are assessed.

In the first case study, the CCGT's power variations following the frequency deviations under different steady-state variations are plotted in Fig. 3. Note that the power and frequency deviations represent variants in the variables P_m and ω_r, respectively. The frequency traces have the same nadir as well as initial rate of change of frequency (RoCoF). In fact, this case study is designed in order to model the frequency responses of a power system with different governor's droop gains.

Indeed, the larger frequency deviation results in larger power reduction. The question is how linear the relation between the frequency and power deviations under diverse frequency excursions is. In order to answer it, let us select the solid traces in Fig. 3 as the base case in order to estimate the power deviations of the other two cases as follows:

$$\Delta P_{ss2} = \frac{\Delta f_{ss2}}{\Delta f_{ss1}} \Delta P_{ss1} \tag{6}$$

where, the subscript *ss* denotes the post-event steady-state condition. The estimated power drop is compared with its true value in Fig. 4. As can be seen, the estimation error increases by moving away from the base case.

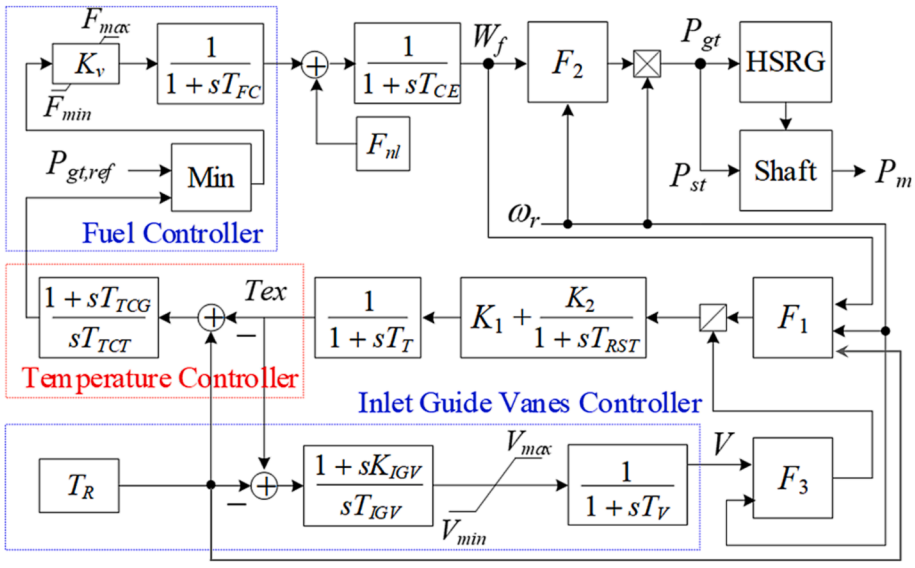

Fig. 1. The block diagrams of the prime mover model for the studied CCGT [5,19].

Table 1
Parameters of The CCGT Power Plant [5,19].

T_{drum}	300	T_{FC}	0.06	T_{CE}	0.45	T_{RST}	15	K_{st}	0.325
K_m	0.15	T_R	950	A	700	T_{TCT}	450	F_{min}	0.15
T_n	3	F_{nl}	0.23	B	550	T_{TCG}	3.3	F_{max}	0.77
T_d	10	T_T	0.5	K_1	0.8	T_{IGV}	20	V_{min}	0.095
K_v	0.77	T_V	3	K_2	0.2	K_{IGV}	4	V_{max}	1

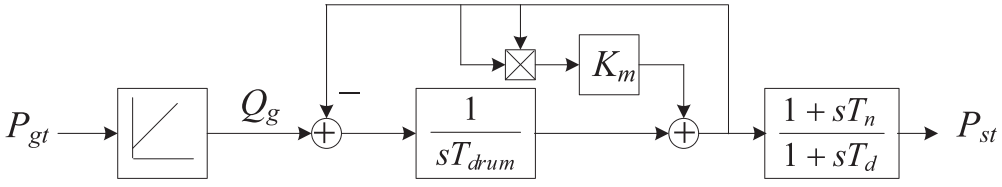

Fig. 2. The block diagrams of the HRSG model [19].

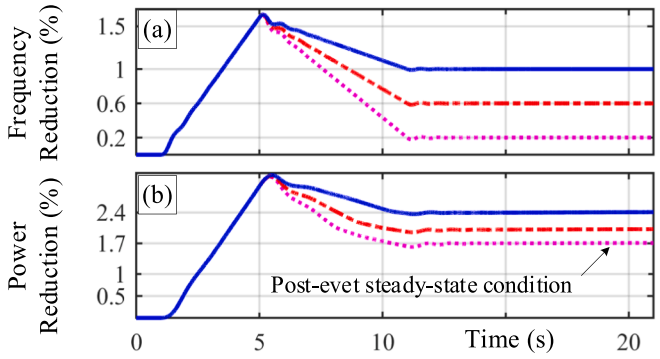

Fig. 3. The CCGT (b) power reductions in response of (a) the frequency reductions with different steady-state frequency variations.

The real-world power systems have the pre-defined governor droop gains. It means that the response to power outages with discrepant sizes is in a roughly identical manner. In other words, the system's frequency changes have similar but scaled shapes for two different disturbances at the whole post-event time. Fig. 5.a shows the three frequency excursions corresponded to the three simulated loss-of-generation events, in

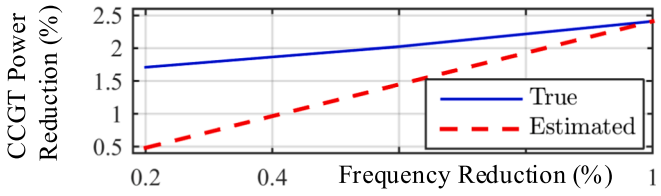

Fig. 4. The true and estimated power reductions of the CCGT based on the steady-state frequency variations (as observed in Fig. 3).

different sizes, to emulate the frequency responses of the real-world power networks. The corresponding CCGT's power reductions are depicted in Fig. 5.b. Hereinafter, if the CCGT's power reduction will be estimated using (6) with the solid traces shown in Fig. 5.a as the base case, the results of Fig. 6 will be obtained. It is clear-cut that the estimation method using (6) works well in the case of the real-world power systems. Before proceeding, it is instructive to intuitively justify the linearity of the observed relationship between the CCGT's power and frequency. As observed, the maximum variations of the frequency illustrated in Fig. 3.a and 5.a are lower than 2 %. Accordingly, the nonlinear behavior of the CCGT model can be approximated by linearization. It is notable that the linearization and thus the estimated power

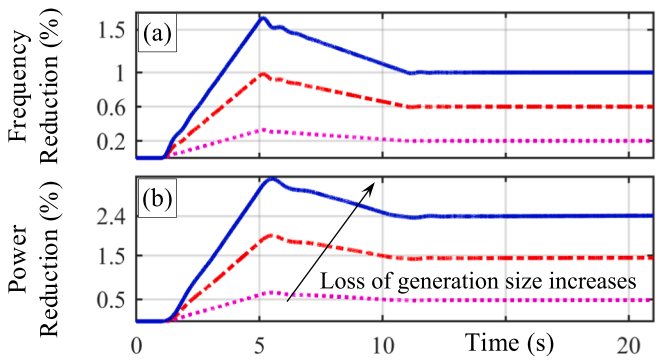

Fig. 5. The CCGT (b) power reductions in response of (a) the frequency reductions with same-shaped frequency deviations.

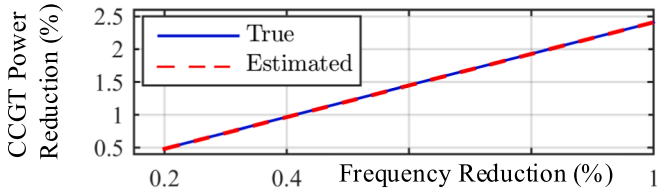

Fig. 6. The true and estimated power reductions of the CCGT versus its frequency reduction based on same-shaped frequency deviations (as observed in Fig. 5).

variation using (6) have negligible estimation error when proportionality between the frequency traces sustains for the entire time interval as depicted in Fig. 5.a. In fact, validity of (6) needs to time-domain proportionality between the frequencies, since there is an integration function in the temperature controller of the CCGT model (see Fig. 1). The gas turbine's exhaust temperature T_{ex}, corresponding with the traces of Fig. 5.a is shown in Fig. 7.a. Following the CCGT's frequency reduction, the exhaust temperature increases due to the compressor's speed reduction. The temperature controller loop mitigates the fuel input to decrease temperature to its rated value 950F. The amount of fuel reduction is proportional with the integral of the exhaust temperature deviation from the rated temperature. This integral are given in Fig. 7.b. it can be observed that the ratios between the traces of this figure are identical with those of Fig. 5.a. The estimated power reduction of the CCGT derived by (6) will be deployed in the next section for more accurate estimation of loss-of-generation size in the power systems including CCGT units.

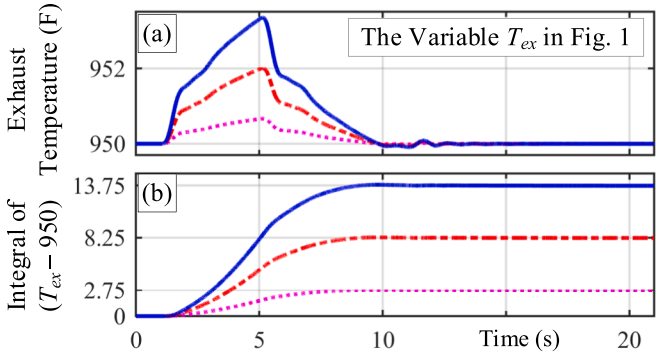

Fig. 7. The CCGT's (a) exhaust temperature and (b) integral of its deviation from the rated temperature 950F.

3. The proposed loss of generation size estimation

In this section, an analytical approach to estimate the loss-of-generation size is presented. Consider a power system with three synchronous generators (SG), the single line diagram of which is illustrated in Fig. 8. Denote the generators active power generation, the loads active power consumption and the transmission lines active power dissipation by P_g, P_l and P_{loss}, respectively. Further, P_1 to P_3 represent active power flow at the end of the lines. Let the generator SG3 be suddenly disconnected at t_0. Denote the time immediately before the tripping SG3 out by t_{0-}, the loads consumption powers are:

$$P_{l1}(t_{0-}) = P_{g1}(t_{0-}) + P_3(t_{0-}) - P_1(t_{0-}) - P_{loss1}(t_{0-})$$

$$P_{l2}(t_{0-}) = P_{g2}(t_{0-}) + P_1(t_{0-}) + P_2(t_{0-})$$

$$P_{l3}(t_{0-}) = P_{log}(t_{0-}) - P_2(t_{0-}) - P_{loss2}(t_{0-}) - P_3(t_{0-}) - P_{loss3}(t_{0-}) \quad (7)$$

in which, the loss-of-generation power is signified by P_{log}. Following the considered power outage event, the above equations set change as follows:

$$P_{l1}(t) = P_{g1}(t) + P_3(t) - P_1(t) - P_{loss1}(t)$$

$$P_{l2}(t) = P_{g2}(t) + P_1(t) + P_2(t)$$

$$P_{l3}(t) = -P_2(t) - P_{loss2}(t) - P_3(t) - P_{loss3}(t) \quad (8)$$

that is valid for

$$t \geqslant t_0 \quad (9)$$

Subtracting (7) from (8), the lost power may be expressed as follows:

$$P_{log}(t_{0-}) = \sum_{i=1}^{2} \Delta P_{gi}(t_1) - \sum_{i=1}^{3} \Delta P_{lossi}(t_1) - \sum_{i=1}^{3} \Delta P_{li}(t_1) \quad (10)$$

wherein,

$$\begin{aligned} \Delta P_{gi}(t) &= P_{gi}(t) - P_{gi}(t_{0-}), i = 1,2 \\ \Delta P_{lossi}(t) &= P_{lossi}(t) - P_{lossi}(t_{0-}), i = 1,2,3 \\ \Delta P_{li}(t) &= P_{li}(t) - P_{li}(t_{0-}), i = 1,2,3 \end{aligned} \quad (11)$$

In other words, the lost power is equal to the total variation in the power generations of the generators subtracted by the cumulative power deviations of the loads and the lines losses.

3.1. Estimation of the variation in power generation

Immediately after a power outage, the online generators increase their electrical power through sacrificing their rotor's speed to compensate the tripped power. This intrinsic response of the SGs is known as inertial response. Following the SGs inertial response, and when the frequency exceeds a pre-defined boundary, the governors increase mechanical power of the SGs proportionally with the frequency reduction. Therefore, the variation in the power generation following an infeed loss event may be written as follows:

$$\Delta P_g(t) = \Delta P_{ir}(t) + \Delta P_{gr}(t) \quad (12)$$

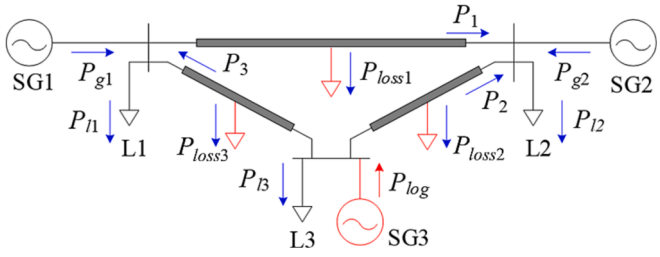

Fig. 8. The single line diagram of the three-machine system.

in that, the total inertial and governor responses are denoted by ΔP_{ir} and ΔP_{gr}, respectively. Let there are n SG units in the power system, the governor's response can be calculated as:

$$\Delta P_{gr}(t) = -\Delta f_{coi}(t)\sum_{i=1}^{n}\frac{P_{pfri}}{R_i} \tag{13}$$

where, parameters R_i and P_{pfri} indicate the governor droop gain and the nominal active power of the i^{th} synchronous generator with primary frequency response (PFR) capability. Further, the center-of-inertia (COI) frequency deviation is:

$$\Delta f_{coi}(t) = f_{coi}(t) - f_{nom} \tag{14}$$

with f_{nom} as the nominal frequency. The COI frequency f_{coi} is defined as follows:

$$f_{coi}(t) = \frac{\sum_{i=1}^{2} H_i S_{bi} f_i(t)}{\sum_{i=1}^{2} H_i S_{bi}} \tag{15}$$

wherein, f_i is the frequency of the i^{th} SG. The inertia constant and base apparent power of the i^{th} SG are represented by H_i and S_{bi}, respectively.

Now, the cumulative inertial power of the SGs can be calculated using their swing equation as [23–25]:

$$\Delta P_{ir}(t) = -\left(\sum_{i=1}^{2} 2H_i S_{bi}\right)\frac{d}{dt} f_{coi}(t) \tag{16}$$

In general, the primary frequency response is delivered completely up to about 15 s following the incident [26]. This is an automatic response, and the system operator does not have sufficient time to optimize it. On the other hand, the secondary frequency control (SFC), which initiates at about 60 s after the disturbance can be optimized based on the reliable estimation of the lost power [27]. Therefore, the disturbance size estimation should be accomplished before the SFC initiation. At this steady-state condition, the derivative of f_{coi} in (16) tends to zero, thus, the inertial response can be ignored in the lost power estimation.

3.2. Estimation of the transmission lines power loss

The dissipated active power in a transmission line can be calculated as follows [20]:

$$P_{loss}(t) = \frac{v_1^2(t) + v_2^2(t) - 2v_1(t)v_2(t)\cos(\theta_1(t) - \theta_2(t))}{\left(R_{line}^{-1} Z_{line}^{2}\right) V_{nom}^{-2}} \tag{17}$$

where v_1 and v_2 denote the end-side voltages of the transmission line in per-unit and, R_{line} and Z_{line} are its resistance and reactance in ohm. Note that the capacitor charging currents are ignored in (17). By taking derivative of the above equation with respect to the line's voltage angles, the variation in the line's power loss can be estimated as:

$$\Delta P_{loss}(t) = \frac{2v_1(t_{0-})v_2(t_{0-})(\sin(\theta_{12}(t_{0-}))\Delta\theta_1(t) - \sin(\theta_{12}(t_{0-}))\Delta\theta_2(t))}{\left(R_{line}^{-1} Z_{line}^{2}\right) V_{nom}^{-2}} \tag{18}$$

with,

$$\theta_{12}(t_{0-}) = \theta_1(t_{0-}) - \theta_2(t_{0-}) \tag{19}$$

3.3. Estimation of deviation in the loads consumption power

From a demand side point of view, the consumption power of the system is the function of system's frequency and voltage. Accordingly, it may be formulated as follows [20]:

$$P_l(t) = \left(1 + k_{pf}\Delta f(t)\right)\left(aPv^{k_{pu0}}(t) + bPv^{k_{pu1}}(t) + cPv^{k_{pu2}}(t)\right)P_{nom} \tag{20}$$

The load damping constant k_{pf} models the frequency dependency of the load's power. This is typically in the range of 0 to 3 [21]. The aP, bP and cP denote the proportion of the constant power loads (CPL), constant current load (CCL) and constant impedance load (CIL) when the parameters k_{pu0}, k_{pu1} and k_{pu2} are set to 0, 1 and 2, respectively. Further, P_{nom} is the nominal power of the load. It can be shown that the deviation of load's power for the small-signal contingencies can be approximated as:

$$\Delta P_l(t) = \begin{pmatrix} 1 + k_{pf}\Delta f(t) + \\ \Delta v(t)\left(aPk_{pu0} + bPk_{pu1} + cPk_{pu2}\right) \end{pmatrix} P_{nom} \tag{21}$$

3.4. Considering the CCGTs power reduction

As exposed in the previous section, the generated power of the full-load CCGT units decreases in response to the system's frequency reduction. This power reduction should be considered in the disturbance size estimation process to make it more precise. As it was revealed in section 2.1, there is a roughly linear relationship between power and frequency reductions of the heavy-duty CCGT units as follows:

$$\Delta P_{ccgt}(t) = -\frac{\Delta f_{coi}(t)}{R_{ccgt}} P_d \tag{22}$$

where, P_d is the system's demand. The parameter R_{ccgt} represents CCGT's droop gain with negative value that is dependent on the PFR characteristic of the power system. Therefore, the equation (10) considering the CCGTs power variation becomes:

$$P_{log}(t_{0-}) = \Delta P_g(t) - \Delta P_{loss}(t) - \Delta P_l(t) + \Delta P_{ccgt}(t) \tag{23}$$

A flowchart illustrating the proposed disturbance size estimation methods is presented in Fig. 9. A disturbance detection technique is used to start the estimation process. The phasor measurement units are located in pre-defined locations to measure the input data of the power system's voltage and frequency. In Method 1, the estimated disturbance size is equal to the total response of the governors. The estimation error is mitigated in Method 2, wherein the variation in the transmission line

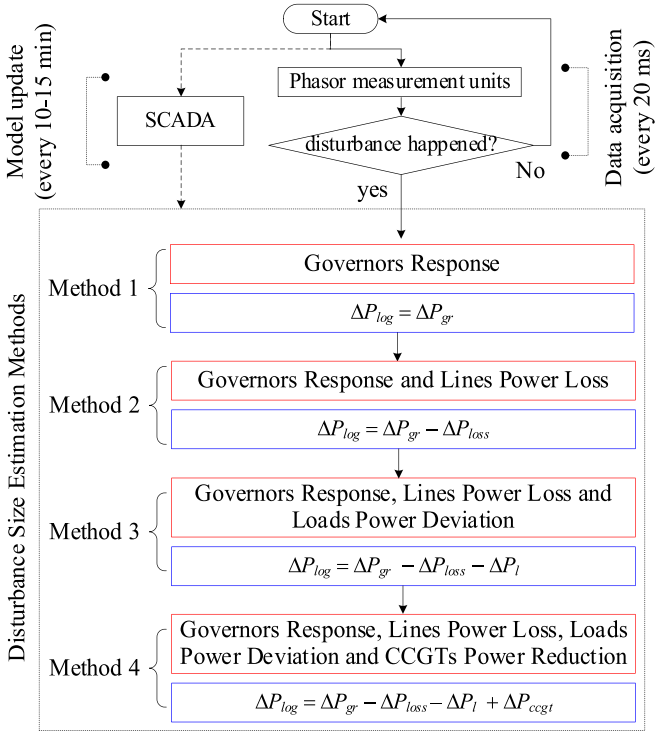

Fig. 9. Flowchart of the proposed disturbance size estimation methods.

losses is considered. In Method 3, the deviation in the load's consumption power is also used in the estimation process along with the lines power loss. Finally, the power reduction of the CCGT power stations is incorporated into the disturbance size estimation in order to achieve more accurate results.

4. Simulation results

In this section, the effectiveness of the suggested approach to estimate size of an infeed loss is investigated using the 36-zone equivalent network representing the national electricity transmission system of Great Britain (GB) power system. The single line diagram of this system which is implemented in DIgSILENT PowerFactory is shown in Fig. 10. The system demand is 40 GW with load damping constant equal to 1. The CPL, CCL and CIL construct 20 %, 35 % and 45 % of the loads, respectively. All the system's demand is supplied by 41 power plants equipped with SGs. These power stations have gas-fueled, nuclear, or hydro turbines with 60,250 MVA total capacity to generate 48 GW of active power. The surplus power is exported to the neighboring countries. The capacity and geographic distribution of the gas-fueled units which generate 29 GW are illustrated in Fig. 10 [28]. Four hydro turbines and one pump storage are located in the Scotland region and generate about 1,700 MW while the other units are nuclear stations. For the sake of simplicity, a simple reheat steam turbine is deployed for all gas and nuclear units [29]. Governors of these units have a 5 % droop. The hydro turbines are modelled as the nonlinear hydraulic turbines in which the output power is controlled by hydraulic governors with 5 % permanent and 20 % temporary droops [22].

Regarding the gas-fueled power plants, three scenarios are defined named "GT scenario", "CCGT scenario" and "GT-CCGT scenario". There is no CCGT unit in the system in the first scenario while it is assumed that all the gas-fueled units are equipped with CCGT technology in the second scenario. As the worst case, all the CCGTs operate in their full-load conditions, however, this is not the case in reality. On the other hand, only 60 % of the gas-fueled units have CCGT technology in the GT-CCGT scenario [1].

In this scenario, gas-fueled units located in zones 4, 10, 12, 16, 20 and 24 are CCGT units and those of the other zones are open-cycle gas turbines. All units except those of zones 10 and 35 participate in frequency regulation. In this context, the frequency-dependent capacity of the grouped power plants for three scenarios is tabulated in Table 2. Here, "Others" group includes all nuclear and hydro units. It is worth to mention that the larger capacity of the gas-fueled group in the CCGT scenario is due to that the generated power of the CCGT units located in zones 10 and 35 can be reduced in response of the frequency reduction incident, however, their governor actions are disabled. The disturbance size estimation is conducted for six contingencies listed in Table 3. These disturbances have deliberately been selected with different sizes, up to about 1,800 MW which is the largest possible infeed loss in GB and National Grid has to ensure system security for them [27].

4.1. The first case Study: The GT scenario

The COI frequency deviations following the considered disturbances are portrayed in Fig. 11. The delivered governor responses of the grouped generation units are also shown in Fig. 12. Hereinafter, all the power variables are represented in percentage of the system's demand, *i.e.*, 40 GW. In the other hand, the post-event deviations in the lines power loss and the system's demand are illustrated in Fig. 13. Both true and estimated values are given in this figure. The estimated traces are calculated using (18) and (21). As observed, it can be inferred that the demand side power deviations are considerable, and the disturbance size estimation error will increase by neglecting them.

The disturbance sizes are estimated at 30 s following the incidents and the obtained estimation errors are illustrated in Fig. 14. In the Method 1, wherein only the governor's response is used, the estimation error ranges from −2% to −8%. Considering the lines power loss in the Method 2, the obtained errors are mitigated for some cases and are increased for the other cases. Finally, Method 3, in which the post-event

Table 2
Frequency-dependent capacity of the grouped power plants.

Units	GTs		CCGTs		Others	
Scenario	MW	%	MW	%	MW	%
GT	24,160	60.4	0	0	18,152	45.4
CCGT	0		29,024	72.6	18,152	45.4
GT-CCGT	11,096	27.7	17,930	44.8	18,152	45.4

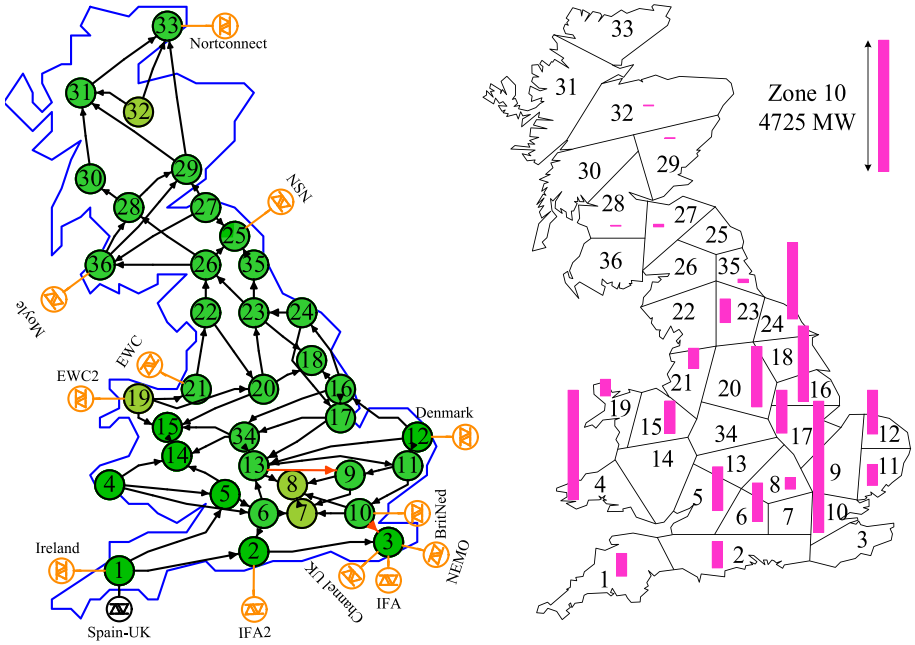

Fig. 10. Schematic of the GB power system implemented in DIgSILENT PowerFactory (left) and the gas-fueled power plants distribution (right).

Table 3
The Simulated Loss of Generation events (Base power is 40 GW).

No.	Unit	MW	%	No.	Unit	MW	%
1	Biomass 27	120	0.3	2	Gas 8	420	1
3	Gas 19	615	1.5	4	Gas 1	808	2
5	Nuclear 3	1300	3.2	6	Biomass 23	1720	4.3

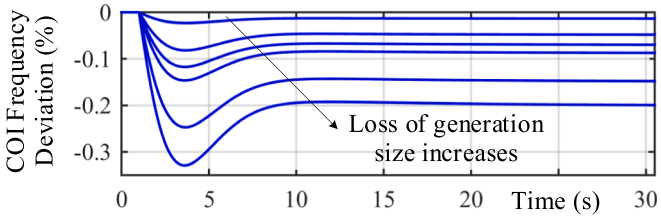

Fig. 11. The COI frequency deviations for the GT scenario.

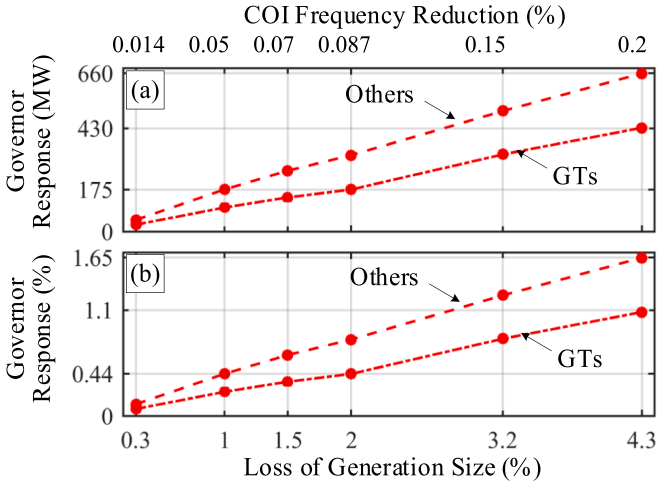

Fig. 12. The governor responses for the GT scenario.

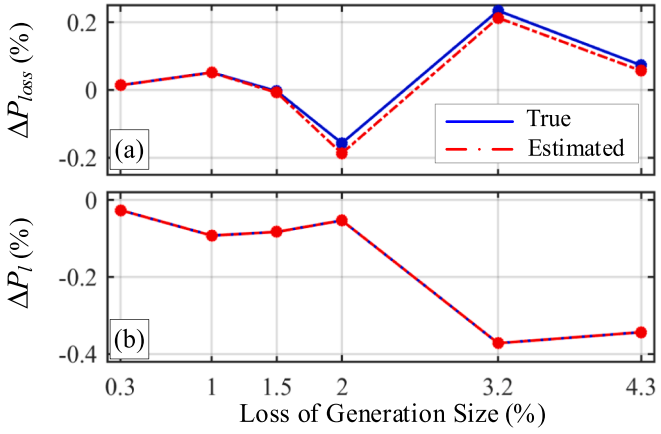

Fig. 13. Post-event deviations in load and loss powers for the GT scenario.

variation of the system's demand is also incorporated into the estimation process works well in comparison with the two previous methods.

4.2. The second case Study: The CCGT scenario

The time-domain COI frequency deviations after the events are portrayed in Fig. 15. The largest frequency nadir and steady-state

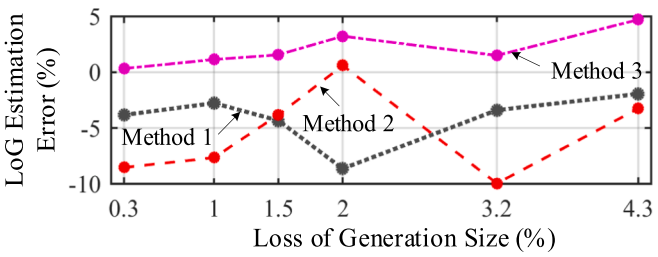

Fig. 14. Errors in loss of generation size estimation for the GT scenario.

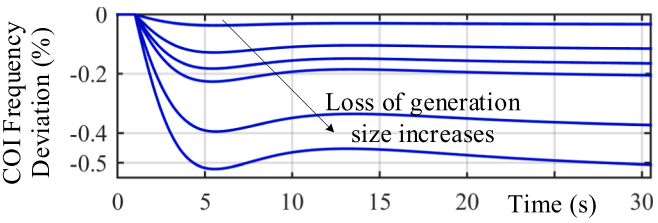

Fig. 15. The COI frequency deviations for the CCGT scenario.

frequency deviation are about 50 % and 150 % more than those of the GT scenario. As previously discussed, this is due to the power reduction of the fully loaded CCGT units in response of the frequency reduction, as shown in Fig. 16. This CCGT's behavior increases the PFR burden on the 'Others' generation units by 160 % in comparison to the GT scenario. Fig. 17 represents the estimated load and loss power deviations. While the power losses are roughly identical with the GT scenario, the load power is gone up by about 150 % in the CCGT scenario due to its greater steady-state frequency deviation. The power-frequency characteristic of the CCGT units is portrayed in Fig. 18. In this case, parameter R_{ccgt} that was introduced in (22) is about −0.75 %. It means the power generation of the CCGTs reduces by 1 % if the system frequency drops by 0.75 %. This parameter is reciprocal of the characteristic's slope. The errors in estimated size of the disturbances are compared for the presented methods in Fig. 19. In contrast with the GT scenario, there is a significant offset estimation error in the case of the Method 3 regardless of the disturbance size. However, this offset error is approximately removed by considering the CCGTs power reduction in the Method 4. Consequently, ignoring the power reduction of the CCGTs has substantial impact on the accuracy of the estimated size of the power outages.

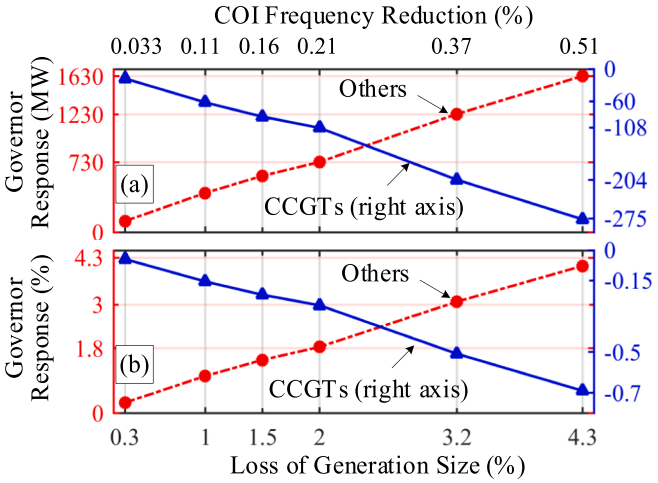

Fig. 16. The governor responses for the CCGT scenario.

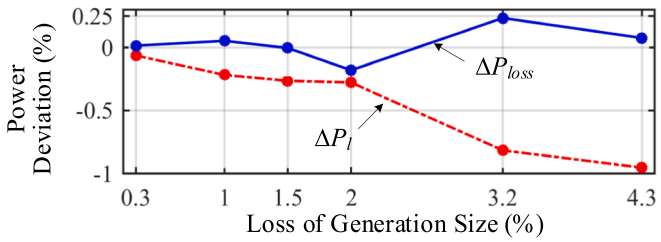

Fig. 17. Post-event deviations in load and loss powers for the CCGT scenario.

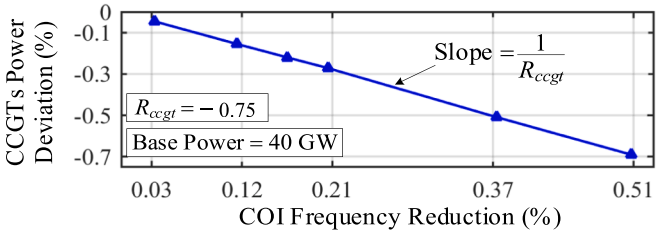

Fig. 18. The CCGTs power-frequency characteristic for the CCGT scenario.

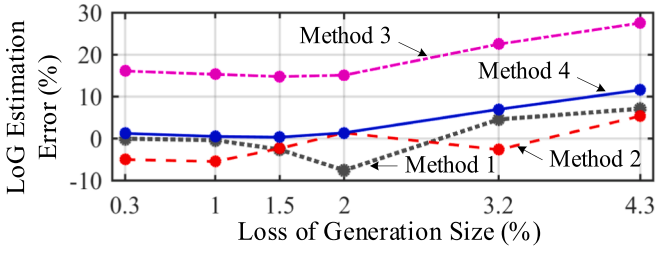

Fig. 19. Errors in loss of generation size estimation for the CCGT scenario.

4.3. The third case Study: The GT-CCGT scenario

In this scenario, the CCGT's contribution in the gas-fueled power stations is reduced from 100 % to 60 % in comparison with the CCGT scenario, which was studied previously. The simulation results of this scenario are portrayed in Figs. 20 to 23. At first glance, the frequency regulation burden on "Others" generation units is mitigated by 35 %, which is in accordance with the reduced contribution of the CCGTs. This relationship can also be observed in the case of parameter R_{ccgt} derived in Figs. 22 and 18. The estimation errors shown in Fig. 23 approve the

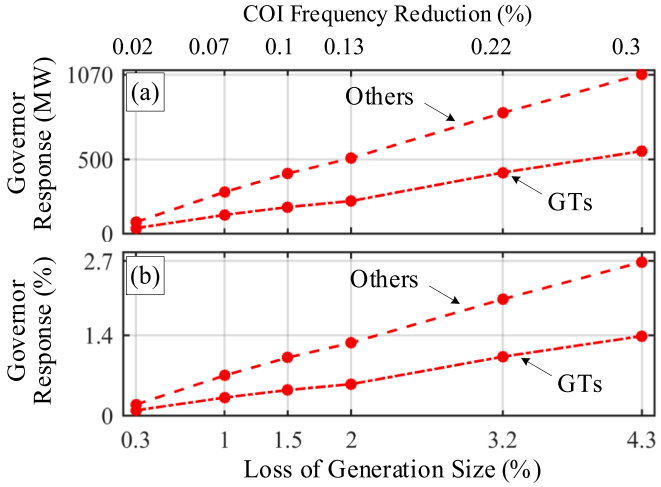

Fig. 20. The governor responses for the GT-CCGT scenario.

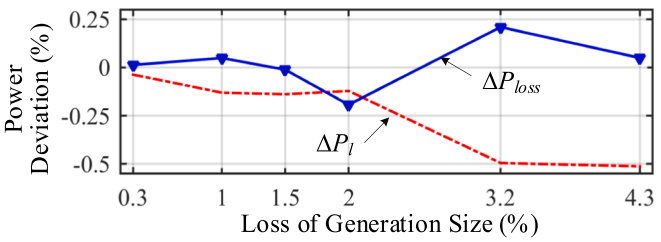

Fig. 21. Post-event deviations in load and loss powers for GT-CCGT scenario.

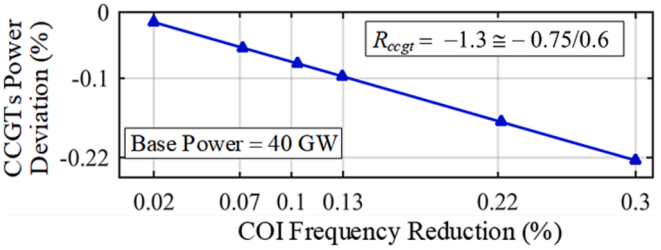

Fig. 22. The CCGTs power-frequency characteristic for GT-CCGT scenario.

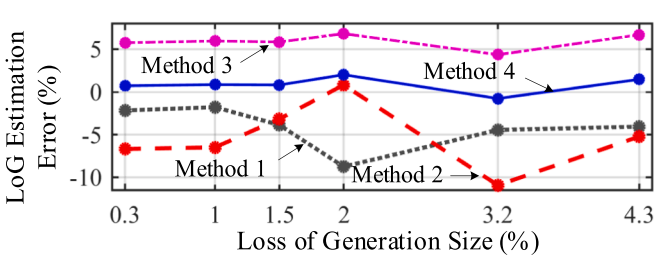

Fig. 23. Errors in loss of generation size estimation for GT-CCGT scenario.

superiority of the Method 4 in comparison with other methods.

Additionally, it is interesting to observe from Fig. 23 that comparable estimation errors of Method 1 with those of Method 4 in Fig. 20 has not a theoretical justification. To better explanation, the cumulative deviations in the system demand and the lines power loss are compared with the CCGTs power deviation in Fig. 24 for both scenarios. In the case of the CCGT scenario, reduction in the CCGTs power is roughly compensated by deviation in the system demand and loss power. Thus, Method 1 works well in this scenario. In other words, this is a special condition, and it is not the case for the GT-CCGT scenario.

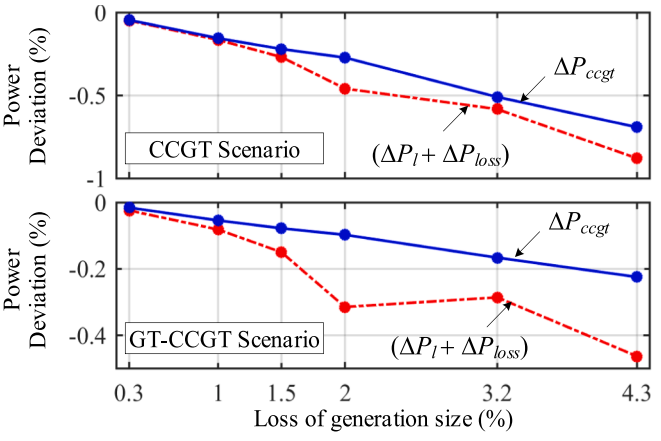

Fig. 24. Comparison of the CCGTs power deviation with the cumulative deviations in the system demand and loss powers.

5. Conclusions

In this paper, the dynamic behavior of the heavy-duty combined cycle gas turbine (CCGT) power plants is initially examined in response to different frequency incidents. It is found out that despite the non-linear dynamic behavior of the CCGTs, there is a roughly linear relationship between the steady-state frequency and power reductions of these plants (in post-event condition) in the real-world power grids. This relationship defines a negative droop gain for the CCGT units. The value of this droop gain depends to the characteristics of the CCGT. Then, a new analytical method to estimate the disturbance size is presented by formulating the power-balance equations in the pre- and post-event conditions. Deviations in post-event demand side consumption in terms of system demand and transmission line losses are also formulated in the proposed approach. Moreover, the CCGT's power-frequency characteristic is derived and added into the primary frequency response equations in order to achieve more accurate disturbance size estimation. The simulation results conducted on an equivalent Great Britain power system indicate that the more precise outage size can be derived using the proposed framework. The observed droop gain for the studied CCGTs was around 0.75 % when all generation units be the CCGTs. It means the power generation of the CCGT reduces by 1 % if the system frequency drops by 0.75 %.

CRediT authorship contribution statement

Rasoul Azizipanah-Abarghooee: Conceptualization, Methodology, Validation, Formal analysis, Writing – original draft, Writing – review & editing, Supervision. **Mostafa Malekpour:** Conceptualization, Methodology, Software, Investigation, Data curation, Writing – original draft. **Rafat Aljarrah:** Writing – review & editing, Visualization. **Mazaher Karimi:** Methodology, Formal analysis, Resources, Writing – original draft, Supervision, Funding acquisition. **Vladimir Terzija:** Writing – review & editing, Project administration.

Declaration of Competing Interest

This research has received generous support from the School of Technology and Innovations at the University of Vaasa.

Data availability

The data that has been used is confidential.

References

[1] UK energy in brief 2018, July 2018, https://assets.publishing. service.gov.uk/government/uploads/system/uploads/attachment_data/file/728374/UK_Energy_in_Brief_2018.pdf, accessed 20 April 2019.
[2] Enhanced Frequency Control Capability (EFCC), October 2014' //www.smarternetworks.org/Files/Enhanced_Frequency_Control_Capability_141125101940.pdf, accessed 01 April 2015.
[3] Gooi HB, Mendes DP, Bell KRW, Kirschen DS. Optimal scheduling of spinning reserve. IEEE Trans Power Syst 1999;14(4):1485–92.
[4] Bruninx K, Van den Bergh K, Delarue E, D'haeseleer W. Optimization and allocation of spinning reserves in a low-carbon framework. IEEE Trans Power Syst 2016;vol. 31(no. 2): p. 872–82.
[5] Lalor G, Ritchie J, Flynn D, O'Malley MJ. The impact of combined-cycle gas turbine short-term dynamics on frequency control. IEEE Trans Power Syst 2005;20(3):1456–64.
[6] Pan K, Guan Y. Data-driven risk-averse stochastic self-scheduling for combined-cycle units. IEEE Trans Ind Informat 2017;13(6):3058–69.
[7] Kakimoto N, Baba K. Performance of gas turbine-based plants during frequency drops. IEEE Trans Power Syst 2003;18(3):1110–5.
[8] Meegahapola L. Characterization of gas turbine dynamics during frequency excursions in power networks. IET Gener Transm Distrib 2014;12(8):1733–43.
[9] Saffarian A, Sanaye-Pasand M. Enhancement of power system stability using adaptive combinational load shedding methods. IEEE Trans Power Syst 2011;26(3):1010–20.
[10] Ketabi A, Hajiakbari Fini M. An underfrequency load shedding scheme for hybrid and multiarea power systems. IEEE Trans Smart Grid 2015;6(1):82–91.
[11] Anderson PM, Mirheydar M. An adaptive method for setting under-frequency load shedding relays. IEEE Trans Power Syst 1992;7(2):647–55.
[12] You H, Vittal V, Yang Z. Self-healing in power systems: An approach using islanding and rate of frequency decline-based load shedding. IEEE Trans Power Syst 2003;18(1):174–81.
[13] Carmona S, Rios S, Pena H, Raineri R, Nakic G. Combined cycle unit controllers modification for improved primary frequency regulation. IEEE Trans Power Syst 2010;25(3):1648–54.
[14] Zografos D, Ghandhari M, Eriksson R. Power system inertia estimation: Utilization of frequency and voltage response after a disturbance. Elect Power Syst Res 2018;161:52–60.
[15] Chen YC, Domínguez-García AD, Sauer PW. Generalized injection shift factors and application to estimation of power flow transients. In: 2014 North American Power Symposium (NAPS), Pullman, WA; 2014. p. 1-5.
[16] Chen YC, Dhople SV, Domínguez-García AD, Sauer PW. Generalized injection shift factors. IEEE Trans Smart Grid 2017;8(5):2071–80.
[17] De Mello FP, Ahner DJ. Dynamic models for combined cycle plants in power system studies. IEEE Trans Power Syst 1994;9(3):1698–708.
[18] Rowen WI. Simplified mathematical representations of heavy-duty gas turbines. J Eng Power 1983;105(4):865–9.
[19] CIGRE Task Force: 'Modeling of gas turbines and steam turbines in combined cycle power plants'; 2003.
[20] Price WW, Taylor CW, Rogers GJ. Standard load models for power flow and dynamic performance simulation. IEEE Trans Power Syst 1995;10(3):1302–13.
[21] Concordia C, Ihara S. Load representation in power system stability studies. IEEE Trans Power App Syst 1982;4:969–77.
[22] Kundur P, Balu NJ, Lauby MG. Power system stability and control. New York: McGraw-hill; 1994.
[23] Wang J, Wang F, Zhang Z, Li S, Rodríguez J. Design and implementation of disturbance compensation-based enhanced robust finite control set predictive torque control for induction motor systems. IEEE Trans Ind Informat 2017;13(5):2645–56.
[24] Mo O, D'Arco S, Suul JA. Evaluation of virtual synchronous machines with dynamic or quasi-stationary machine models. IEEE Trans Ind Electron 2017;64(7):5952–62.
[25] He L, Li Y, Shuai Z, Guerrero JM, Cao Y, Wen M, et al. A flexible power control strategy for hybrid AC/DC zones of shipboard power system with distributed energy storages. IEEE Trans Ind Informat 2018.
[26] Sharma S, Huang SH, Sarma ND. "System inertial frequency response estimation and impact of renewable resources in ERCOT interconnection", IEEE PES. GEM 2011:1–6.
[27] National Grid. NETS Security and Quality of Supply Standard, version 2.2, 2012. [Online]. Available: http://www2.nationalgrid.com /UK/Industryinformation/Electricity-codes/SQSS/The-SQSS/.
[28] National Grid, Distribution Network Operator (DNO) Companies Available: http://www2.nationalgrid.com/UK/Ourcompany/Electricity/ Distribution-Network-Operator-Companies/, 2017.
[29] Anderson PM, Mirheydar M. A low-order system frequency response model. IEEE Trans Power Syst 1990;5(3):720–9.